



ASCE

# Investigation into the Internal Erosion and Local Settlement of Esfarayen Earth-Fill Dam

Seyyed Kazem Razavi<sup>1</sup>; Masoud Hajialilue Bonab<sup>2</sup>; and Ahmad Dabaghian<sup>3</sup>

**Abstract:** A considerable sudden settlement was discovered on the Esfarayen Earth-fill Dam surface near to the left abutment when the reservoir level rose to 51 m from the riverbed in April 2013. As a result, a detection process was prepared to comprehend the problem and relevant challenges required to consider devising an appropriate remedial work. For this purpose, the work was divided into three main parts: (1) analyzing the information gathered from the monitoring and surveillance plan, (2) performing a geotechnical site investigation to test the subsurface condition and the extent of the problem, and (3) finding the cause of the problem initiation by considering three aspects—the bedrock geological condition, material susceptibility, and three-dimensional numerical modeling. The outcomes from the different parts of the study categorized the problem as an internal erosion incident. The existence of an inadequate sealed crushed zone of a fault passing through the reservoir on the contact surface with the clay core was the major cause of the internal erosion initiation. The water, appearing through this narrow crushed zone, applied additional hydrostatic pressure on the clay core, which depended on the reservoir level and had no influence on the stress distribution inside the dam. With the water pressure exceeding the minor principal total stress, a crack formed and extended with time, turning to a large void. Because of the high quality of the clay core material and its well-designed downstream filter, the internal erosion progression was concentrated on the core and directed to the upstream. When it reached the upstream filter, the filter entered into the core, and the material from the overlying part of the dam repeatedly dropped, resulting in a final settlement on the dam surface. The numerical modeling was successful in the determination of the approximate time of the internal erosion initiation by considering the past loading history of the dam and the influence of the existing defect. DOI: [10.1061/\(ASCE\)GT.1943-5606.0002216](https://doi.org/10.1061/(ASCE)GT.1943-5606.0002216). © 2020 American Society of Civil Engineers.

**Author keywords:** Internal erosion; Earth-fill dam; Detection; Numerical modeling; Geotechnical investigation.

## Introduction

Earth-fill dams have provided a range of environmental, economic, and social benefits for thousands of years. For these structures, the phenomenon, known as internal erosion, is an important potential failure mode according to the statistics of the history of failures and incidents (MacGregor et al. 2014). Overall, about 0.55% (1 in 180) embankment dams have failed due to internal erosion, and 1% (1 in 100) embankment dams have experienced an internal erosion incident (MacGregor et al. 2014; Foster et al. 2000a, b). Therefore, it is necessary to study all the similar case studies to advance our knowledge in dealing with such a life-threatening event (Flores-Berrones et al. 2011; Yea et al. 2013; Gillon 2014). This paper introduces a case study subjected to an internal erosion incident and the measures applied to find the problem.

The study consists of three main parts. The first part focuses on the presence of some problems in the dam revealed through the monitoring and surveillance plan. The second part assesses the dam

safety by the discovery of the extent of the problem using conventional site investigation methods, such as drilling boreholes around the affected zone. The third part concentrates on finding the cause of the internal erosion initiation. According to Garner and Fannin (2010), the initiation and progression of the internal erosion require the presence and interaction of the following three factors: (1) material susceptibility, (2) critical stress conditions, and (3) critical hydraulic load. For the material susceptibility, the internal instability of the alluvial foundation (Rönnqvist and Wiklander 2014; Wan and Fell 2008), filter incompatibility (FEMA 2011; USBR 2011), separation of individual clay particles, and its dispersivity potential are assessed using modern techniques. In addition, a geological study has been conducted to characterize the defects of the bedrock. A refined three-dimensional numerical modeling has been performed to determine the low-stress zone and hydraulic gradient inside the dam body. The numerical model established in this study uses a two-phase approach for the core elements to simulate the construction pore pressure generation and its consolidation effect. The Duncan and Chang (1970) constitutive model is written in C++ code and loaded to the Flac 3D software to simulate the nonlinearity of the material. The applicability of the model is verified by comparing the numerical total stress and settlement with the measured ones. After carefully investigating all the collected information, the influential scenario is explained to consider designing an appropriate remediation plan.

## Esfarayen Earth Fill Dam and Detection of the Problem

Note. This manuscript was submitted on December 3, 2018; approved on October 23, 2019; published online on February 4, 2020. Discussion period open until July 4, 2020; separate discussions must be submitted for individual papers. This paper is part of the *Journal of Geotechnical and Geoenvironmental Engineering*, © ASCE, ISSN 1090-0241.

The Esfarayen Dam is located about 19 km to the northeast of Esfarayen, North Khorasan, Iran. The latitude of the dam is 37.080113°, and the longitude is 57.641130°. It is a typical

earth-fill dam with an inclined clay core, filter zone, sandy gravel shell, and rock-fill. It has a crest length of 104 m and a height of 64 m from the riverbed, which was constructed in one year between 2003 and 2004 in a narrow valley. Fig. 1 illustrates the structural details of the dam body. During the visual inspection of the dam in April 2013, a considerable and sudden settlement shown in Fig. 2 was observed on the dam surface near to the left abutment when the reservoir level rose to 51 m from the riverbed. The reservoir level decreased from that time and never exceeded 25 m from the riverbed. As part of the surveillance plan, the detection process concentrated on the monitoring data and the quality of the water in the drainage system.

### Investigation of the Monitoring Data

Three sections named C, F, and H illustrated in Fig. 1 were instrumented with total pressure cells, electrical piezometers, standpipes, settlement gauges, and inclinometers to monitor the behavior of the Esfarayen Dam. Fig. 3 illustrates the location of some electrical piezometers in section H. The instrument name was labeled with the following format: type of the instrument + name of the section representing its location + the number assigned for it. For example, EPH9 and EPF9 represented the ninth electrical piezometers installed at sections H and F, respectively, and FPH1 was the identification for the first electrical piezometer installed at section H in the bedrock or alluvial foundation. It must be mentioned that the

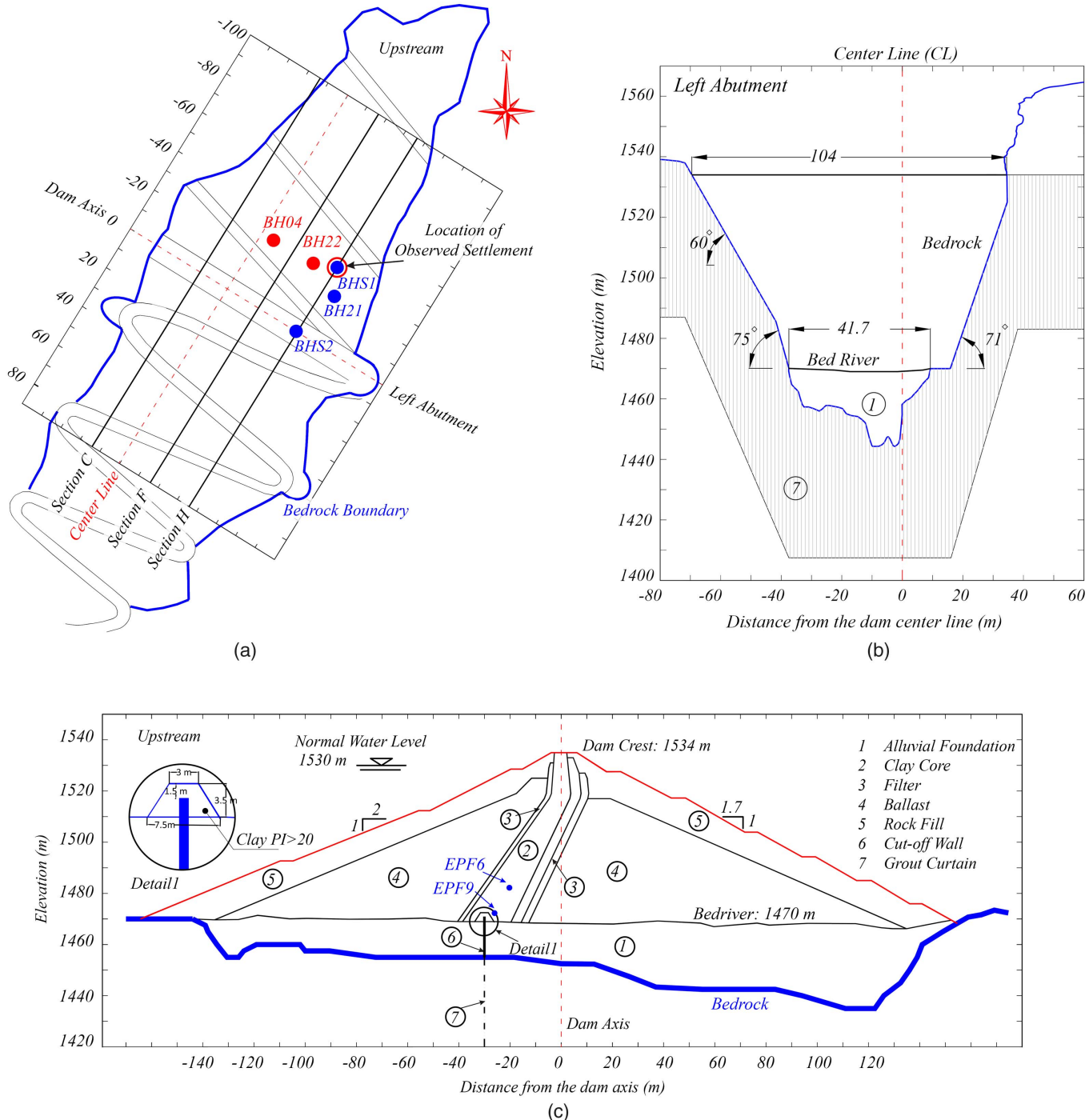
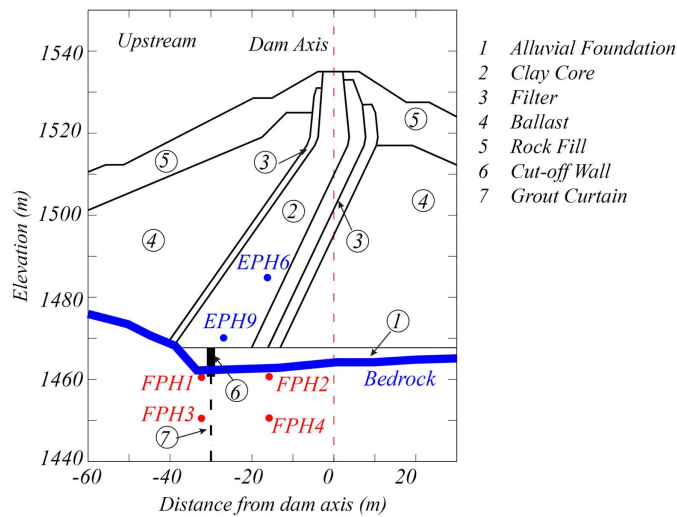


Fig. 1. Esfarayen earth-fill dam—structural details.



**Fig. 2.** Observed surface settlement near to the left abutment. (Map data © 2019 Google, Image © 2019 Maxar Technologies.)



**Fig. 3.** Location of some electrical piezometers at section H-H.

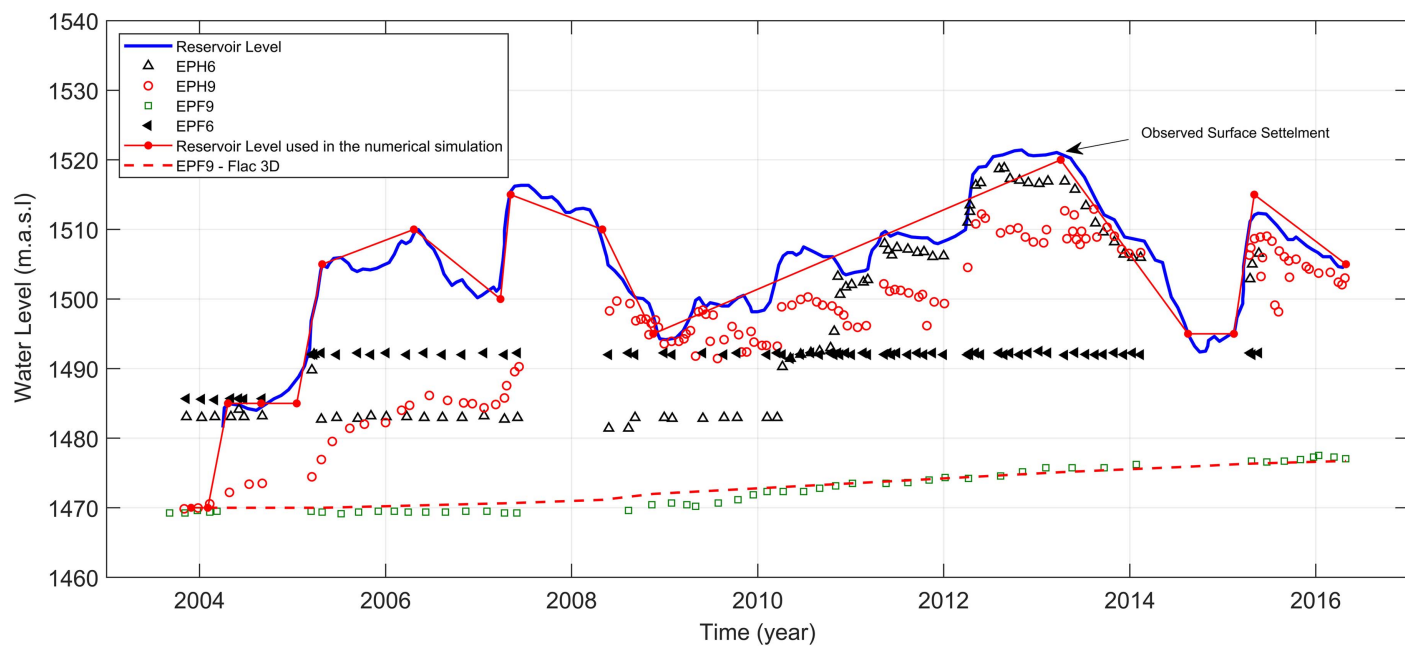


**Fig. 4.** Pore water pressure recorded for EPH6, EPH9, EPF9, and the monitored reservoir level.

original instrumentation was installed at the same elevation and location relative to the core geometry in both section H-H and F-F, and therefore, the EPH9 and EPF9 recorded data, for example, could be compared with each other.

By reviewing all the monitored data, the corresponding electrical piezometers installed in the clay core manifested a remarkably different trend in pore water pressure (PWP) changes in section H. Fig. 4 shows the monitored data for EPH6, EPH9, EPF6, EPF9, the reservoir level, and the time of visual detection of the considerable settlement. It is noticeable from the figure that the EPH9 was influenced by the reservoir level fluctuation from the beginning of the reservoir impounding, and the PWP rose, becoming equal to the reservoir level in December 2008. While the PWP monitored at EPF9 confirmed no considerable changes under the reservoir level fluctuation. The EPH6 also exhibited the same trend similar to EPH9 after two and a half years, while the corresponding instrument in other sections presented no notable changes in PWP. As a result, in section H and at elevation 1,472–1,473 m (located near EPH9), a weakness must have existed, resulting in the rapid changes of PWP and extending gradually in time to elevation 1,485–1,486 m (located near EPH6).

The purpose of the electrical piezometers named FPH1 to FPH4, illustrated in Fig. 3, was to investigate the cut-off wall and grout curtain effectiveness in section H. Fig. 5 shows the PWP changes recorded in these instruments in comparison with the reservoir level fluctuations. It can be seen that instruments FPH1 and FPH3 were influenced by reservoir level fluctuations in the left abutment, while the pore pressure variation in the FPH2 and FPH4 were insignificant, showing that the cut-off wall and the grout curtain were able to show their role in the water-tightness of the bedrock. Also, it is mentionable that the PWP monitored at all the instruments installed downstream of the clay core, cut-off wall, and grout curtain showed no noteworthy changes over time due to the reservoir level fluctuations.

#### Checking and Testing of Downstream Water Quality Samples

For the evaluation of material transport by seepage flow as a sign of internal erosion, water samples were collected from the drainage

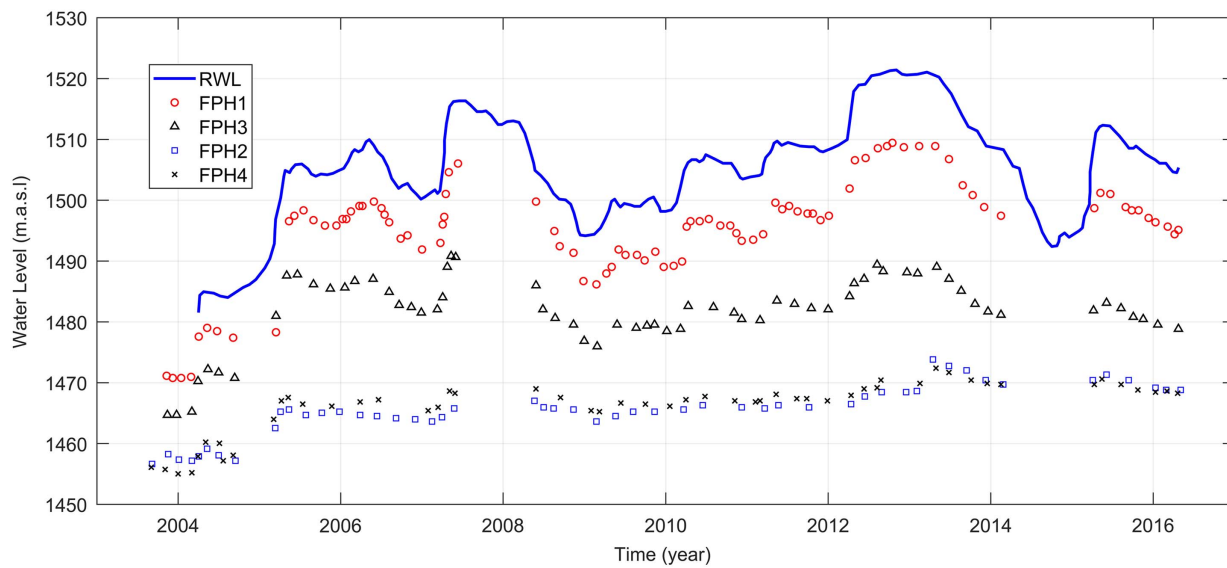


**Fig. 5.** Pore water pressure recorded for FPH1, FPH2, FPH3, and FPH4 with the monitored reservoir level.

system in the downstream once per week for 5 months. The turbidity and total suspended solids (TSS) test were performed based on ASTM D1889 (ASTM 2000) and ASTM D5907 (ASTM 2003), respectively. The variation of the TSS (average value = 0.0 ppm) and turbidity (average value = 2.2 NTU) over this time was insignificant; there was no sign of eroded clay core material in the samples based on the visual inspection during sampling.

### Determining the Extent of the Problem

An immediate subsurface exploration around the damaged zone was performed to find out the conditions of the materials, the extent of the problem, and the causes of the incident. This information will be used for planning and designing the new rehabilitation and site improvement method. The investigation consisted of drilling five boreholes [BHS1, BHS2, BH04, BH21, and BH22 in Fig. 1(a)] in the dam body to obtain undisturbed soil samples. BHS1, BH21, and BHS2 are alongside section H, while BH21, BH22, and BH04 are parallel to the dam axis in the longitudinal direction, as illustrated in Fig. 1. Table 1 shows the boreholes information used in the study. The core drilling and sampling were conducted based on ASTM 2312 (ASTM 2011a) using a single tube core barrel in soil and double tube core barrel in bedrock. Additionally, no drilling fluid was used during drilling to avoid any possibility of hydraulic fracturing.

BHS1 was drilled vertically at the center of the observed settlement. The borehole manifested the following findings regarding the

changes in the position and physical properties of the dam body material. The location of these changes is shown schematically in Fig. 6 and are as follows: (1) the original boundary of the rock-fill with the ballast material and the filter position was displaced downward about 2.71 and 3.88 m, respectively; (2) the filter material was in mixture with the clay core or with the fines part of the ballast material; (3) during the sampling in the clay core, some part of the extracted soil was soft and saturated. The title of softened clay is used in this study to show their location in Fig. 6. Also, it was expected that one drill 12.87 m in the clay core based on the as-built drawings. Nonetheless, the length of drilling was 7.6 m; and (4) above the alluvial foundation, there was 1–2 m stiff clay.

BH21 revealed a two-meter rod fall at elevation 1,475 m, as shown in Fig. 6. Ten meters above the rod fall, the clay core took its liquid form. The saturation for the Lefranc test setup was not possible for this area, which showed a high permeability.

The boreholes BH22 and BH04 determined the extent of the problem in the longitudinal direction. In Fig. 7, the values of the standard penetration test (SPT) conducted on the clay core material for three boreholes (BH21, BH22, and BH04) are shown. As can be seen, the SPT value in BH22 and BH04 was high and ranged from 20 to 25, while in BH21, it ranged from 7 to 13, showing strength loss around this borehole. In addition, the clay core showed very low permeability in BH22 and BH04 ( $1 \times 10^{-7}$  cm/s). Therefore, the affected area must be limited from the left abutment to section H and from elevation 1,470–1,490 m in the clay core, as shown in Fig. 7.

**Table 1.** Boreholes information used in subsurface exploration in the Esfaryen earth-fill dam

Borehole	Depth	Angle from north	Angle from vertical axis	Drilling in bedrock	Drilling in alluvial foundation	Drilling in dam body	X	Y	Z
BHS1	62.2		Vertical	5.5	5.5	51.5	557,035	4,103,945	1,519
BHS2	57.0	32	22	—	—	57.0	557,014	4,103,915	1,534
BH02	95.4	123	25	77.3	—	18.1	557,042.1	4,103,955.9	1,525.93
BH03	60	123	20	43.1	—	16.9	557,039.2	4,103,926.6	1,526.16
BH04	62.5		Vertical	—	6	56.5	557,006.9	4,103,957.7	1,524.1
BH21	82.5		Vertical	57	—	25.5	557,033.6	4,103,932.4	1,528.12
BH22	80		Vertical	10.9	13.2	55.9	557,024.4	4,103,946.8	1,523.5

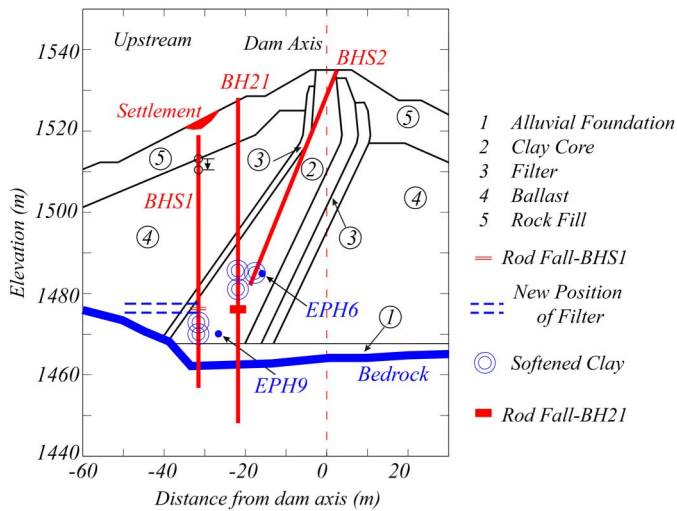


**Fig. 6.** Location and direction of BHS1, BHS2, and BH21 at section H.

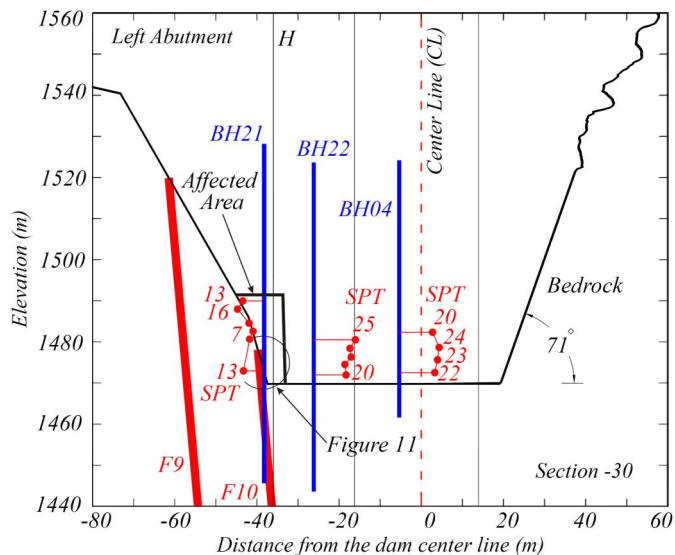


**Fig. 7.** Standard penetration test value conducted on the clay core material in BH21, BH22, and BH04.

## Finding the Cause of the Internal Erosion Initiation

By considering all the information outlined in the previous sections, the conclusion is that an internal erosion was initiated from the core-alluvium contact or the rock-core contact. Its extent concentrated at section H elevation 1,470–1,472 m extended to the upper elevations gradually. Now, the attention is to detect the cause resulting in the initiation of erosion. For this purpose, the study focuses on the geological condition of the bedrock, material susceptibility, and three-dimensional numerical modeling to investigate the low-stress zone and the possibility of hydraulic fracturing.

## Geological Condition of the Bedrock

The Esfarayen Dam was constructed in the sedimentary rocks of the Alborz geo-structural zone based upon the classification of structural domains of Iran (Nabavi 1976). As shown in Fig. 8, geologically, the site of the dam consists of the following: (1) cretaceous limestone with a thick-bedded layer that has a Tigran

formation (KT), and (2) quaternary alluvium, which consists of young terraces (Qt) and channel fill deposits (Qal). There are more than 10 faults at the dam site based on primary studies, such as a field survey. Fig. 8 shows the faults alignment, clay core boundary, grout curtain axis, and the cut-off wall location relative to the geological map of the dam. Before the dam construction, a large amount of bedrock was removed to modify the slope of the abutments and avoid differential settlement and resultant cracking of the earth-fill core. Fig. 9 illustrates the bedrock topography after the bedrock foundation treatment, and in applying dental concrete, notes were recorded from surveys during construction. The bedrock also was covered with a 10 cm layer of shotcrete in its connection with the clay core.

From Figs. 8 and 9, the affected area in the clay core was in connection with the outcropping faults F9 and F10 in some elevations. To characterize the features of the mentioned faults, the authors drilled two inclined boreholes named BH02 and BH03, whose location is shown in Fig. 8. Fig. 10 illustrates the direction of the BH02 with the rock quality designation (RQD) and its Lugeon value. The rock quality designation (RQD) for the F9 and F10 crushed zones is around 40 and 10, respectively, while their Lugeon is almost 50 and 100, respectively. BH21 is also intersected by the F10 crushed zone in contact with the clay core at elevation 1,472 m. The rock samples obtained from that area, shown in Fig. 11, were covered with the clay core material. In this area, the saturation for the Lefranc test setup was not possible, showing its high permeability. Additionally, there was no sign of shotcrete in the clay core-bedrock contact, which intensifies the possibility of the erosion (or scour) of the core into a crushed zone in the bedrock.

## Material Susceptibility Analysis

In this section, the properties of the materials used to build the dam, such as filter, clay core, ballast, and the alluvial foundation, are assessed to evaluate the possibility of the erosion pathway from two aspects: material stability and filter criteria. The first aspect employs laboratory tests and advanced empirical methods to study the internal instability potential of each material. If the material is stable, the filter assessment must consider the as-placed gradation. Otherwise, the conditions required to make the material unstable are reviewed. If there are such conditions, the filter assessment must consider the altered gradations after fines removal.

## Material Internal Instability

**Clay Core.** Dispersive soils are important because erosion could initiate in them under very low hydraulic stress and gradient, and its presence in the soil must be determined if it includes more than 15% fines. The pinhole test [ASTM D4647 (ASTM 1998)] and double hydrometer test [ASTM 4221 (ASTM 2011b)] are the most common laboratory test used to define this property adequately. At least 20 samples from the clay core for each test were examined. Both tests indicated that the clay core was nondispersible to slightly dispersive. To assess the internal instability of the clay core, Wan and Fell (2008) and Fell and Fry (2013) suggest that suffusion does not occur in the existence of the following conditions: (1) a soil plasticity index (PI) > 7 and a hydraulic gradient < 4; and (2) a soil plasticity index (PI) > 12 and a hydraulic gradient > 4. The PI of the Esfarayen clay core varied from 13 to 20 and was not gap-graded; therefore, it is an internally stable material.

**Downstream Filter.** The downstream filter of the Esfarayen Dam has been designed in accordance with the International Commission on Large Dams' (ICOLD) *Embankment Dams Granular Filter and Drains, Bulletin 5* (ICOLD 1994), and its grading curve is drawn in Fig. 12 with the clay core, alluvial foundation, and

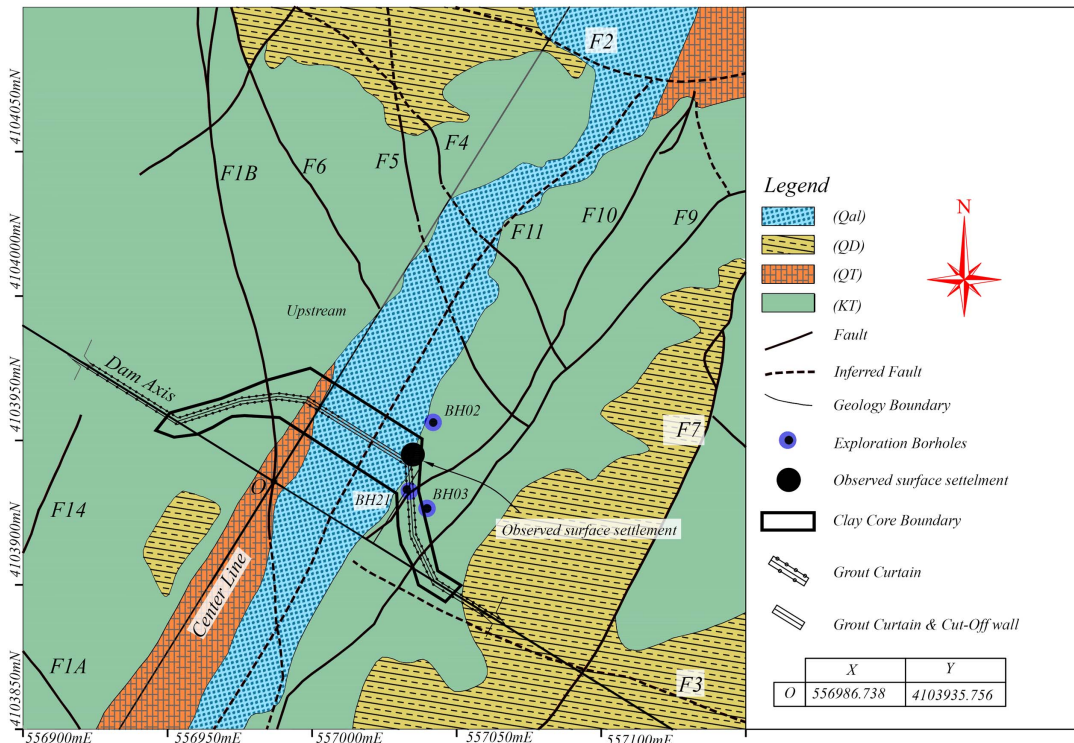


Fig. 8. Geological map of the dam site.

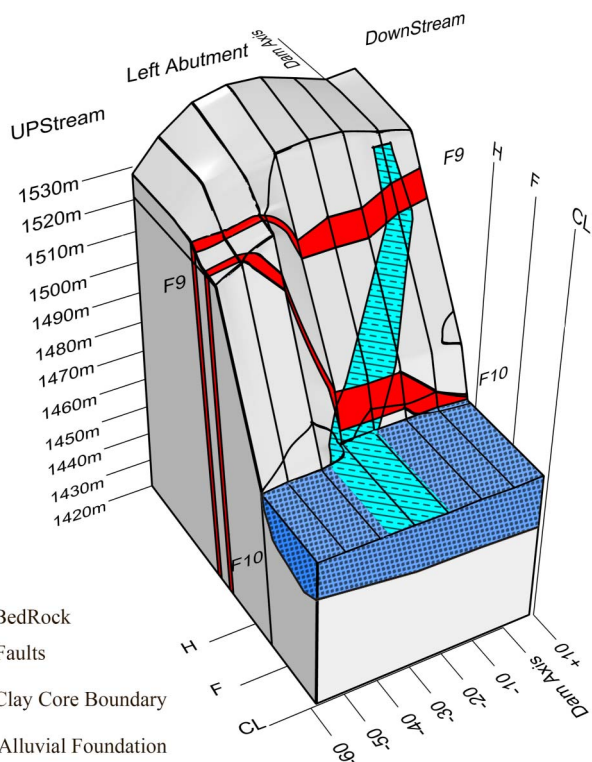


Fig. 9. Bedrock topography after foundation treatment and applying dental concrete.

ballast grading curve. Its gradation curve satisfies the requirements of the USBR (2011) introduced for the filter design. Therefore, it is not gap-graded and meets the particle retention requirements.

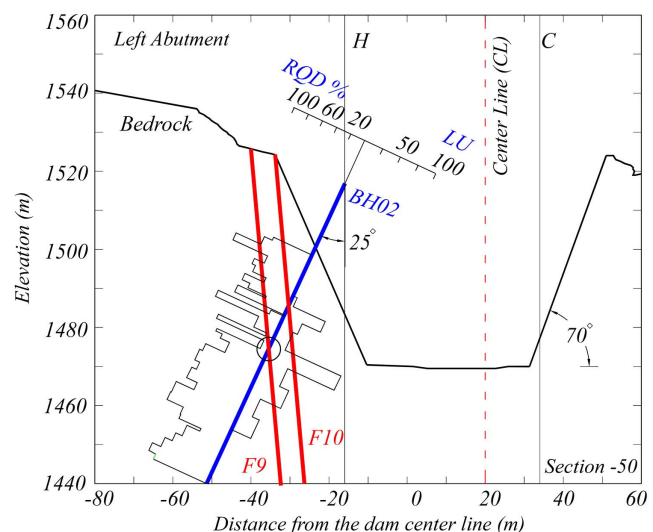


Fig. 10. Rock quality designation and Lugeon value in the direction of BH02.

**Ballast and Alluvial Foundation.** The grading curve of the ballast material and alluvial foundation are wide-graded, as shown in Fig. 12. One of the conventional methods to assess the instability of these soils is the method introduced by Kenney and Lau (1985). The method plots  $F$ , the mass fraction, versus grain size  $D$ . From this,  $F$  versus  $H$ , the mass fraction between  $D$  and  $4D$ , is plotted. Fig. 13(a) shows how the method works. If the soil plots to the left of the boundary ( $H = F$  or  $H = 1.2 F$ ), as shown in Fig. 13(b), its grading is categorized as an unstable grading. Additionally, Fig. 13(b) presents  $H = 0.68F$  suggested by Rönnqvist et al. (2017), which is a more accurate criterion. As can be seen, the ballast and alluvial foundation material are internally unstable.



**Fig. 11.** Rock samples covered with the clay core obtained at elevation 1,475 m.

## Filter Assessment

**Clay Core (Base Soil) to Downstream Filter.** Because of the following two main reasons, the downstream filter of the Esfarayen Dam was successful in preventing the migration of the fines from the base soil. Firstly, it was designed based on the ICOLD (1994), Bulletin 5, in which its gradation curve satisfies the USBR (2011) requirements for the filter. Therefore, if the clay core particles could migrate to the downstream, they could seal the filter. Consequently, it forced the progression of the internal erosion to the upstream side. Secondly, as mentioned earlier, there was no trace of eroded clay core material in the water samples collected from the drainage system in the downstream for the water quality tests.

**Clay Core (Base Soil) to Alluvial Foundation (Filter Rule).** The clay core of the Esfarayen Dam as a base soil is also in contact with the alluvial foundation. Although the alluvial foundation is an unstable material, it experiences high vertical stress due to the dam's body weight. According to the study by Moffat and Fannin (2011), high vertical effective stress in an unstable soil increases the required hydraulic gradient to initiate the suffusion. The high hydraulic gradient could not be developed from the early days of dam operation when the pore water pressure instruments revealed the first signs of internal erosion. Therefore, its as-placed gradation is used to assess its filter rule. The filter and drainage criterion introduced by the USBR (2011) requirements were  $D15_{\text{coarse-side filter}}/d85_{\text{fine-side base soil}} \leq 4$  and  $D15_{\text{fine-side filter}}/d15_{\text{coarse-side base soil}} \geq 4$ , respectively. Fig. 12 shows the filter requirement needed for the clay core as a base soil satisfied by the alluvial foundation. However, if there was a possibility for the erosion of the clay core into the alluvial foundation, it could be a secondary effect. It is likely that the fault provided higher hydraulic gradients near section H leading to erosion of the material into the alluvium.

**Downstream Filter (Base Soil) to Downstream Ballast (Filter Rule).** The grading curve for the downstream ballast material is similar to the alluvial foundation grading curve, as shown in Fig. 12(b). As explained earlier, the fines part of such materials requires a high gradient to provide enough flow velocity to erode. High gradients were not able to develop in the downstream ballast during the dam's operation time, and there is no need to eliminate its fine particles. The downstream filter as a base soil has particles

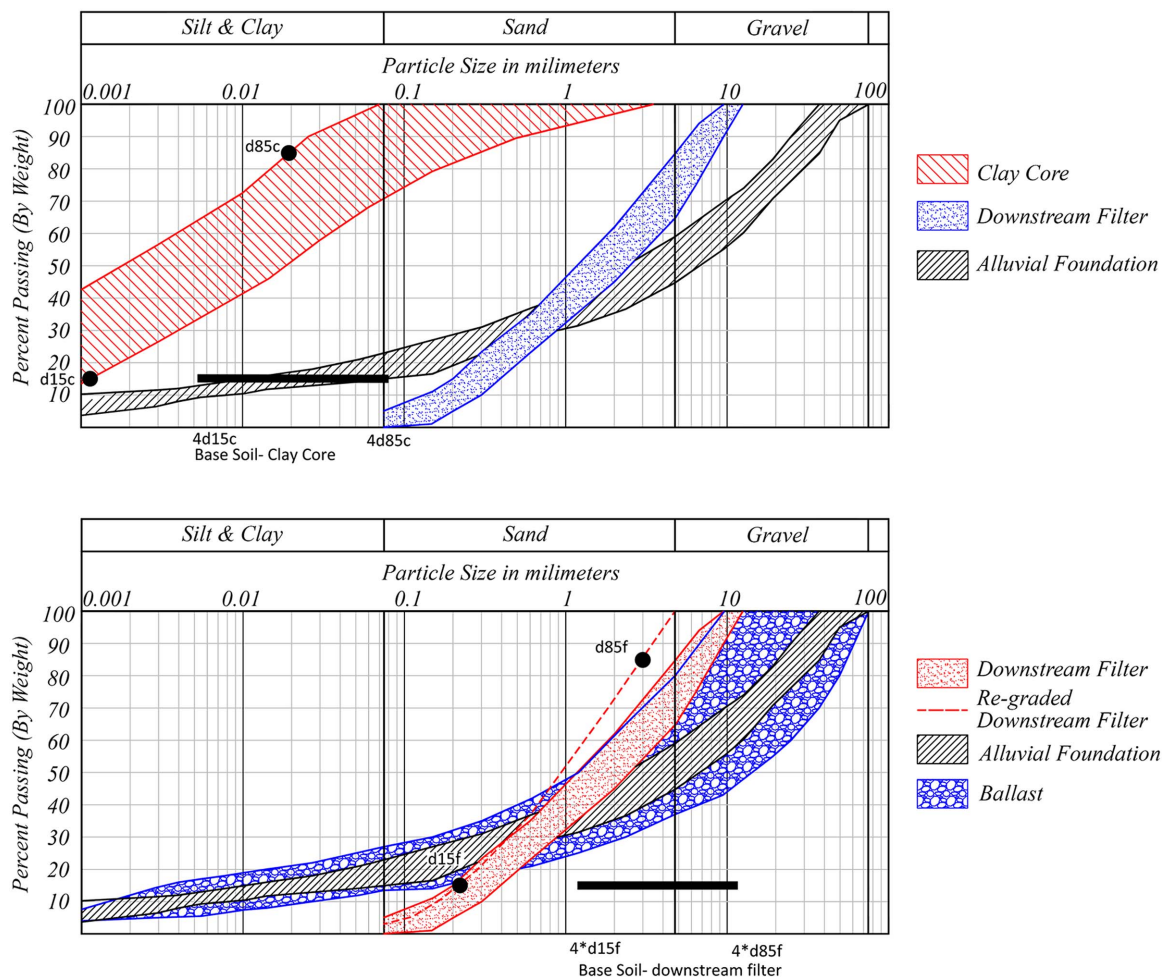


**Fig. 12.** Grading curve of downstream filter, alluvial foundation, ballast, and clay core materials.

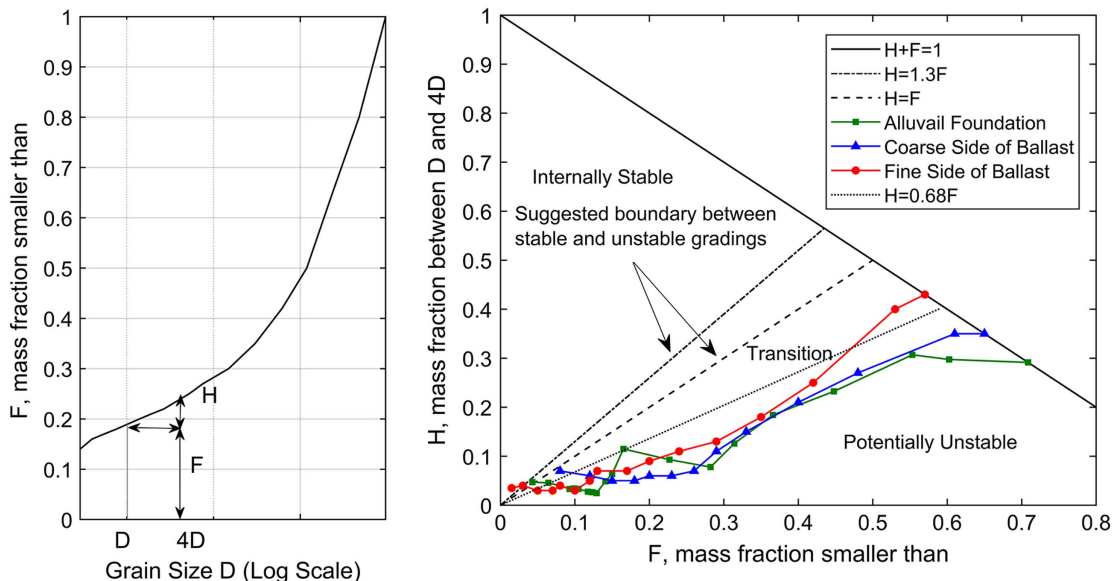


**Fig. 13.** Assessing the internal instability of the alluvial foundation and ballast material by the proposed method of Kenney and Lau (1985).

larger than the No. 4 sieve, and it must be regraded. By doing so, it is obvious that the effective  $d_{15}$  of the ballast material is smaller than four times the  $d_{85}$  of the regraded filter, as shown in Fig. 12(b). As a result, the ballast material satisfies the particle retention (internal stability) requirement as a filter, according to the USBR (2011).

#### Flow Limiting Action of the Upstream Ballast

The ballast gradation shown in Fig. 12 is close to the soil gradations used in the laboratory test by Correia dos Santos et al. (2017) to assess the flow-limiting action of an upstream material. According to their work, as a general rule, soils with plastic fines seem to be associated with a higher likelihood of being effective at limiting the flow. The plasticity index of the ballast material in the Esfaryen Dam varies from 5 to 7, and it has 13% to 25% fines.

#### Numerical Modeling

A hydraulic fracture in soils is a phenomenon whereby the water pressure exceeds the sum of the minor principal total stress and the tensile strength. Numerical modeling (Costa and Alonso 2009) can be employed to investigate the influence of the exact bedrock geometry and simulate the stress-strain behavior of the dam body under a variety of loadings to find the low-stress zones most likely to a hydraulic fracture occurring. To this end, this study uses the commercial software Flac 3D as a three-dimensional explicit finite difference program [Flac 3D (Itasca 2011)] whose application was verified for different boundary value problems by many researchers (Hajialilue-Bonab and Razavi 2016; Razavi and Bonab 2017). Fig. 14 illustrates the discretization of the three-dimensional geometry of the dam body. An interface element is considered between the flexible dam body and the solid neighboring rock to model the soil-structure interaction, including sliding and separation, correctly. Concerning the boundary condition, there is no rationale to consider a long distance from the dam body to the bedrock boundary. Because the bedrock is extremely solid in comparison with the dam body soils, its deformation level would be insignificant.

To simulate the soil nonlinearity behavior, the Duncan and Chang model is used in this study because its parameters are relatively simple and have clear physical meaning (Stark and

Vettel 1991). The constitutive model is implemented into Flac 3D using C++ programming language. The material properties, except for the rock-fill, are calibrated using the results of the laboratory tests performed at the time of the dam's construction, and the new direct shear tests and triaxial tests conducted on the soil samples from the geotechnical site investigations are explained. For example, Fig. 15 shows the simulated stress-strain behavior of the clay core with the triaxial drained compression tests at different confining pressure values. Table 2 lists the material properties used in the Esfaryen Dam.

The past loading history of the Esfaryen Dam can be classified into two main phases. Phase 1 includes the construction of the dam in which almost 80%–90% of the total settlement takes place (Hunter and Fell 2003), and consequently, the stresses developed in the construction stages mostly control the likelihood of low-stress zones and cracking.

The thirteen height increments of thickness equal to 5 m are utilized to simulate the stage construction process. Each increment fill is modeled by activating the corresponding mesh and assigning the soil model and its density based on the embankment construction curve shown in Fig. 16. In each stage, a common two-steps procedure is considered to simulate the construction pore pressure generation and consolidation behavior. First, an undrained analysis is performed to simulate the construction pore pressure generation. Second, until the next fill, drainage is allowed by applying the isotropic Darcy's transport law and considering the clay core/filter interface as a permeable boundary in which fluid flows to and from the outside. The solution to this consolidation problem is expressed in the framework of the Biot theory. Table 2 shows the hydraulic properties of the clay core material. The quality control tests carried out during the construction stage indicated that the core material from elevation 1,470–1,491 m was compacted in a water content of 0.5%–1.5% lower than the optimum water content, and as a result, its saturation degree was low during compaction. Consequently, the amount of construction pore pressure generation can be ignored. However, the core material compacted higher than elevation 1,491 m was quite close to full saturation on placement, and one must consider the two-steps procedure.

Phase 2 includes the impounding and fluctuation of the reservoir level from 2004 to 2017 based on Fig. 4.

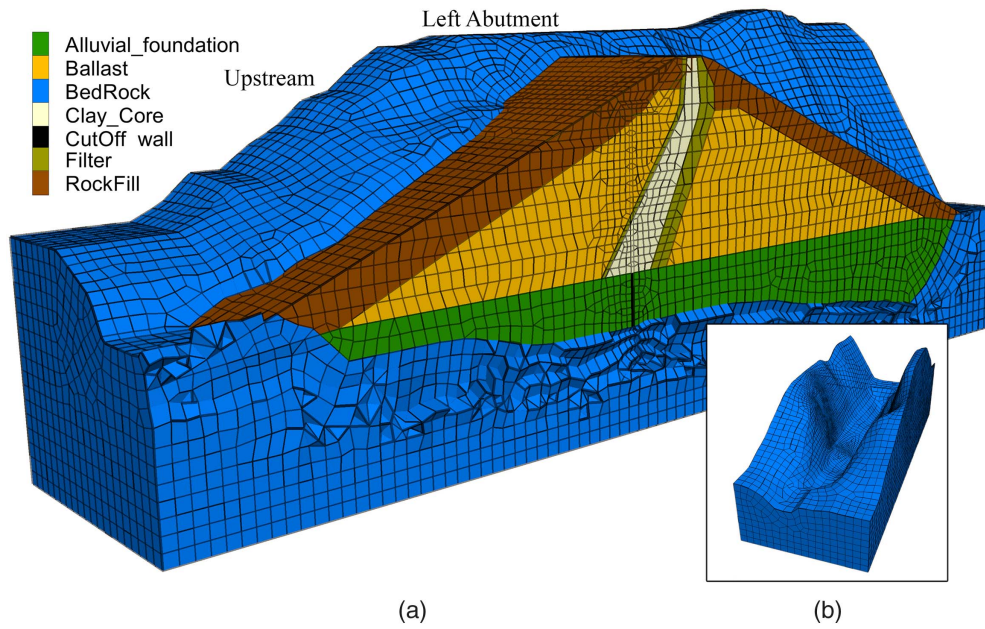


**Fig. 14.** Discretization of the three dimensional geometry of (a) the cutting section F through the dam body; and (b) the bedrock.

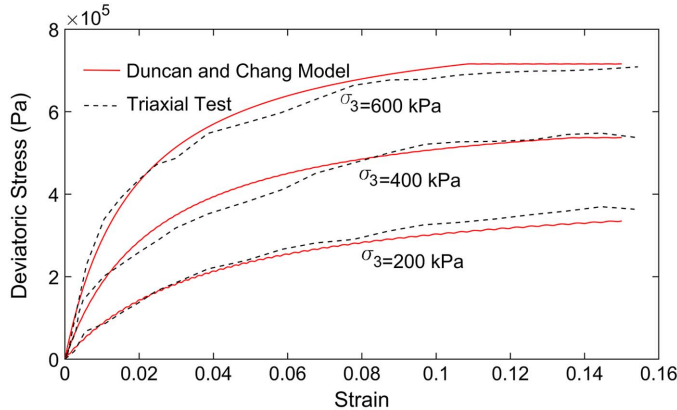


**Fig. 15.** Drained triaxial test on clay core; comparison of experimental results with numerical results.

#### Verification of the Numerical Model

Fig. 17 compares the measured and computed settlements for VSD-F1, VSDF2, and VSDF3 at the end of construction. Fig. 18 illustrates a comparison between the measured and computed total

vertical stress for individual points at elevation 1,471.2 and 1,484.5 m in Section F. The total pressure cells were used to record the total vertical stresses during construction. There is a reasonable agreement between the field-measured data and those computed using the numerical model from two different aspects, including displacement and stress development. The reservoir level fluctuation showed in Fig. 4 is used to simulate the transient flow and pore pressure generation inside the dam body. Fig. 4 shows a comparison between the numerical results of pore pressure at EPF9 with the measured one.

#### Investigation of the Hydraulic Fracture Possibility

Three important points based on the conclusions discussed in the previous sections must be considered to properly investigate the hydraulic fracture possibility:

- The discoveries from the geotechnical investigation showed that the location of the damaged zone is in the clay core between the left abutment and section H from elevation 1,470–1,490 m. Consequently, the attention in this area would be to examine the hydraulic fracture possibility.
- There were two faults named F9 and F10 passing through the reservoir and advancing past the left abutment, and their crushed

**Table 2.** Mechanical and hydraulical properties of the materials used in the Esfaryen earth-fill dam

Dam body material	$K^a$	$n^a$	$Kur^a$	$Kb^a$	$M^a$	$Rf^a$	$\varphi^a$	$\Delta\varphi^a$	$C^a$	$E^b$	$\nu^b$	$\gamma_d^c$	$\gamma_{sat}^c$	$k^d$
Rockfill	1,000	0.25	1,200	370	0.2	0.7	50	10	0	—	—	2,100	2,310	$1 \times 10^{-1}$
Ballast	1,100	0.55	1,300	440	0.2	0.84	39	0	0	—	—	2,100	2,250	$1 \times 10^{-4}$
Filter	400	0.3	600	200	0.2	0.7	35	0	0	—	—	1,900	2,200	$1 \times 10^{-5}$
Clay core	43	1.3	52	50	0.2	0.85	18	0	$65 \times 10^3$	—	—	1,850	2,160	$3.5 \times 10^{-7}$
Alluvial foundation	833	0.3	1,000	700	0.1	0.85	40	0	0	—	—	2,000	2,300	$1 \times 10^{-4}$
Bed rock	—	—	—	—	—	—	—	—	—	$16 \times 10^9$	0.25	2,300	—	—
Cut-off wall	—	—	—	—	—	—	—	—	—	$3 \times 10^7$	0.25	2,100	—	$1 \times 10^{-8}$

<sup>a</sup>Duncan and Chang soil constitutive properties:  $K$  = elastic modulus number;  $n$  = elastic modulus exponent;  $Kur$  = modulus number associated with unloading and reloading;  $Kb$  = bulk modulus number;  $m$  = bulk modulus exponent;  $Rf$  = failure ratio;  $\varphi$  = effective friction angle (degree);  $\Delta\varphi$  = degree; and  $c$  = effective cohesion ( $N/m^2$ ).

<sup>b</sup>Elastic constitutive properties:  $E$  = elastic modulus ( $N/m^2$ ); and  $\nu$  = Poisson ratio.

<sup>c</sup>Material's density:  $\gamma_d$  = dry specific weight ( $kg/m^3$ ); and  $\gamma_{sat}$  = dry specific weight ( $kg/m^3$ ).

<sup>d</sup>Hydraulical properties of the materials:  $k$  = hydraulic permeability ( $cm/s$ ).

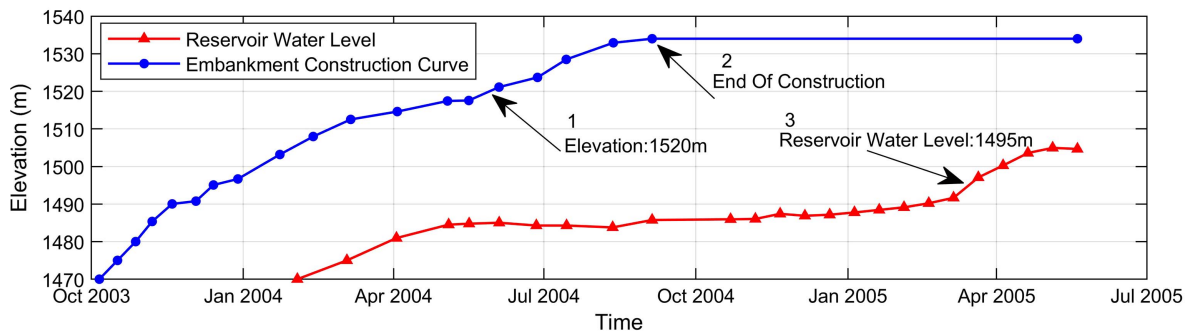


**Fig. 16.** Embankment construction and RWL fluctuation over time.

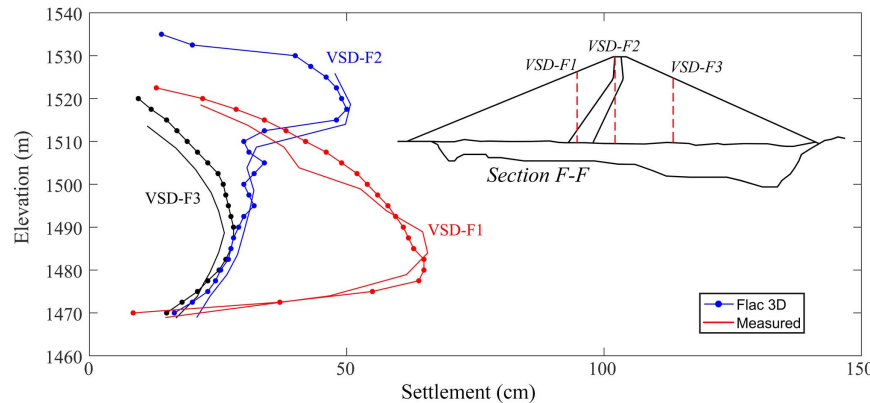


**Fig. 17.** Computed versus measured settlements in different instruments at the end of construction.

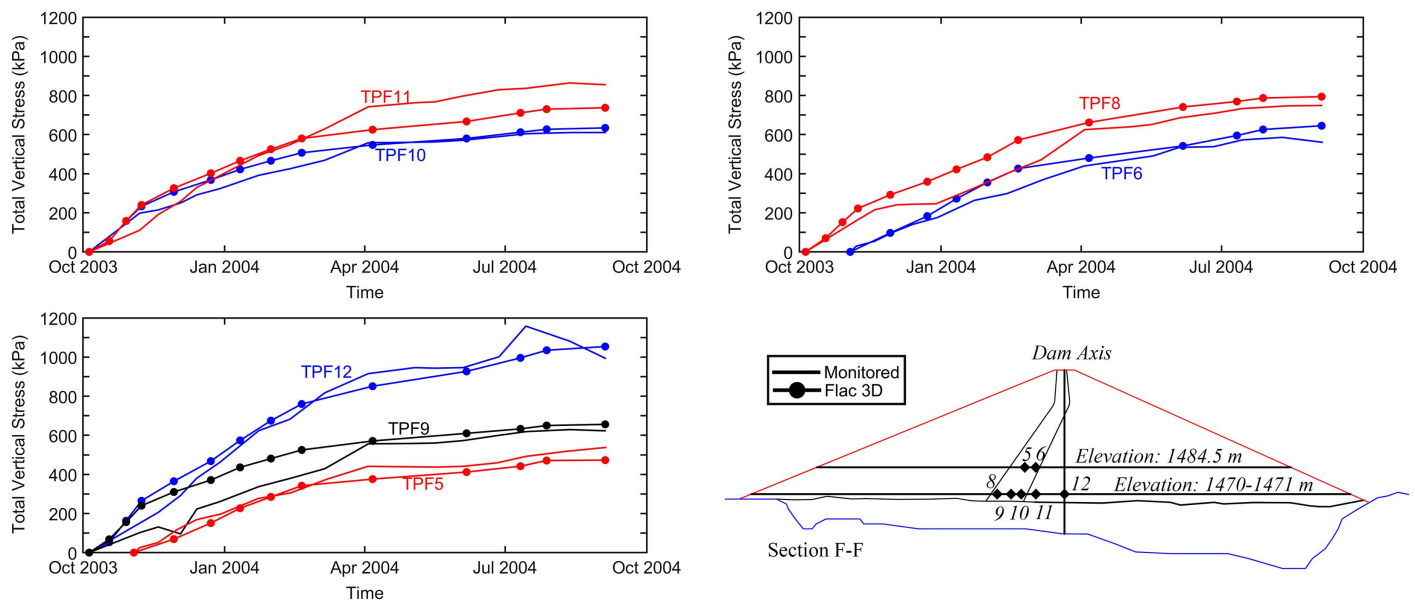


**Fig. 18.** Computed versus measured total vertical stress in the TPF5, TPF06, and TPF08 to TPF12 during the dam construction.

zone after bedrock treatment was in complete contact with the clay core, as illustrated in Fig. 9. The findings also showed high permeability in this area, no sign of the shotcrete layer, and the coverage of the rock samples with the clay core material. Therefore, the reservoir level fluctuation could create an additional

hydrostatic water pressure on the clay core contact through these faults. Because this water pressure is applied through a narrow zone, it has no influence on the stress distribution on the clay core. As a result, it is enough only to compare the calculated additional hydrostatic water pressure based on the reservoir

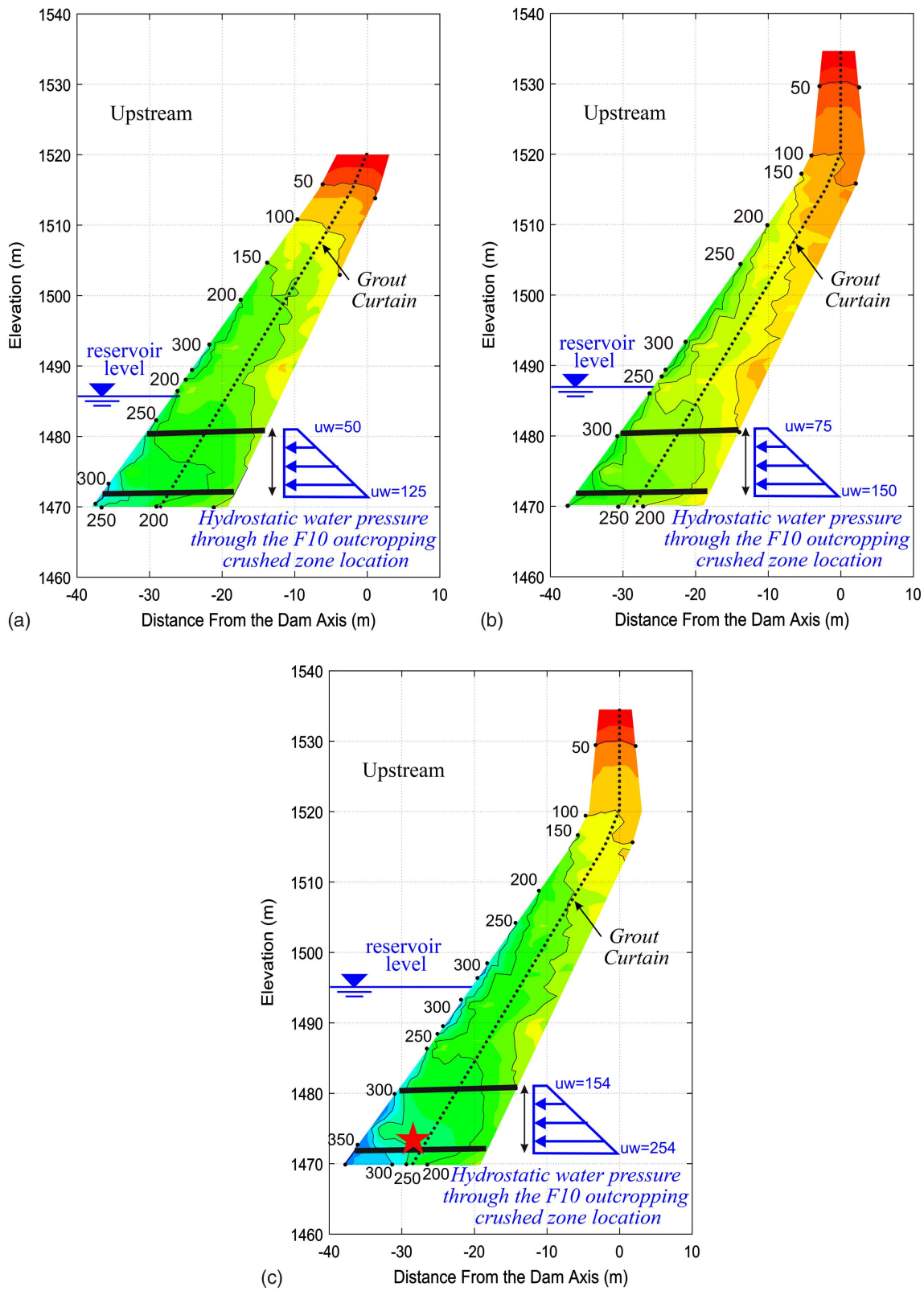


**Fig. 19.** Total minor stress (kPa) at (a) Date 1 (during construction, dam elevation: 1,520 and reservoir level elevation: 1,485 m); (b) at Date 2 (end of construction, reservoir level elevation: 1,485 m); and (c) at Date 3 (reservoir level elevation: 1,495 m).

- level with the internal total minor principal stress in order to control the hydraulic fracture possibility.
- The last months near to the end of dam construction and the first months of reservoir impounding are relevant to the internal

erosion initiation based on the monitored data interpretation discussed previously. As a result, the possibility of hydraulic fracture occurrence needs to be analyzed at this period of time. Fig. 16 illustrates three specific dates. In Date 1, the dam height

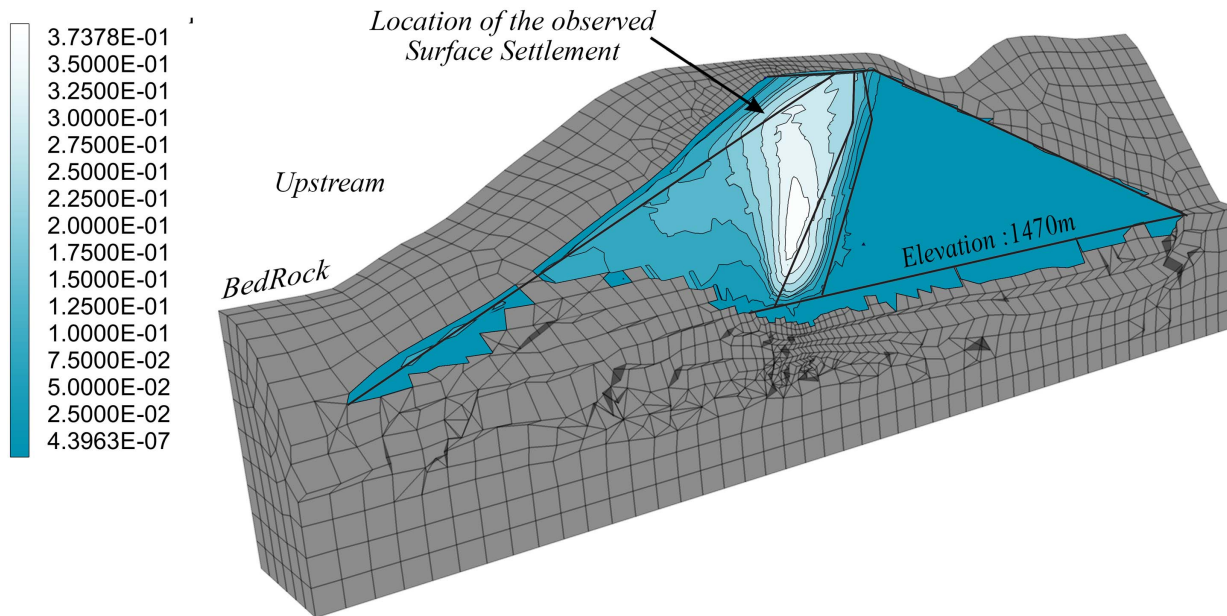


**Fig. 20.** Settlement pattern at Section H in April 2013 when the reservoir level rose to 1,521 m, and the surface settlement had been observed, assuming no internal erosion inside the clay core.

was at elevation 1,520 m, and the reservoir level rose to elevation 1,485 m in June 2004. Date 2 represents the end of the dam construction in September 2004, and Date 3 is when the reservoir level reached to elevation 1,495 m in March 2005.

Fig. 19 shows the minor principal total stress distribution developed in the clay core contact with the left abutment for the three specified dates. The figure also illustrates the hydrostatic water pressure generated by the reservoir level through the outcropping of the F10 crushed zone. As can be seen, the water pressure is lower than the minor principal total stress until Date 3. In Date 3, the hydraulic fracture could initiate in the area shown in Fig. 19(c) by a star.

It is mentionable that there are no susceptible zones to hydraulic fracture occurrence in the case where the contact part between the clay core and the left abutment is impermeable. Fig. 20 shows the vertical settlement pattern for such a case in April 2013, where the surface settlement was observed. The deformation pattern is under the influence of bedrock geometry. As can be seen from Fig. 1, the shape of the valley is much wider and deeper from the longitudinal section –35 m to the dam axis. Therefore, the dam body deformation during impounding is high for this area, which is noticeable in Fig. 20. Therefore, the combination of such inherent settlement of the dam during reservoir fluctuation with the effects of the internal erosion had led to such a sudden final settlement observed in the Esfarayen Dam.

## Discussion

By studying all the data gathered through the geotechnical and geological investigation, material susceptibility, and numerical modeling, the erosion incident appears to be a case of erosion into the foundation (either the core material into the alluvium, the core material into the fault zone, or perhaps a combination of both). The evidence to emphasize the idea of erosion into the alluvium was not as strong as the explorations found to highlight the suggestion of erosion into the fault zone.

Based on the new site investigation and geological study, it is found that some part of the clay core was in direct contact with an outcropping crushed zone in the left abutment, which resulted in additional hydrostatic pressure on the clay core. Because this water pressure was coming through a narrow zone inside the bedrock, it had no significant influence on the stress distribution inside the dam body. Based on the numerical simulation, when the reservoir level rose to 1,495 m, the mentioned water pressure exceeded the minor principal total stress at elevation 1,472–1,475 m, leading to the creation of a crack inside the core. Its signs were recorded with EPH9. By the time the crack opened, it had turned into a large void through washing the clay core particles into the crushed zone (Fig. 11). Subsequently, the upper clay parts lost their strength, ending up with cracking and increasing their permeability. The penetration rate of water into the clay core increased, leading to a sharp rise of pore water pressure in upper elevations. Its signs were recorded with EPH6. From the numerical simulation, the inherent settlement pattern of the dam due to the reservoir level fluctuation intensified the dam body deformation into the eroded area. Thus, when the reservoir level rose to 51 m from the riverbed, the void was not able to hold its roof, and the collapse was activated. With the filter entering, the overlying material was repeatedly dropped, resulting in a sinkhole or a final settlement on the dam surface.

## Conclusion and Recommendations

The main conclusions drawn from this dam incident are the following:

- It illustrated the importance of carefully watching the monitoring data, especially during the first 5 years of operation.
- Lessons learned from this case study show the significance of the bedrock sealing in its contact surface with the clay core, and it is highly recommended to consider a blanket grouting to completely seal this area, especially when a fault is coming from the reservoir.
- Although the downstream filter is very successful in controlling the internal erosion, its function is completely dependant on the

- internal stability of the downstream shell in the case of a developing high hydraulic gradient.
- The response of the Esfarayen Dam, since its construction up until the sudden local surface settlement, was simulated by the Duncan and Chang model, considering the complex geometry of the dam. The numerical analysis was shown to reproduce the overall behavior of the dam to assess the hydraulic fracture possibility well.
  - The construction of a new plastic cutoff wall is a feasible solution to allow this type of dam to operate and meet its original purposes appropriately. Additionally, to prevent any further settlement due to the presence of a soft clay core in the affected area, its mechanical properties can be improved by the ground improvement techniques, such as jet grouting or compaction grouting.

## Acknowledgments

The authors wish to acknowledge the North Khorasan Water Organization, the Toosab Company, the Ghalb company, Ashnab Consulting Engineers, and ANO Consulting Engineers for their support to provide data for this research. The authors also wish to thank Ali Khoshravan Azar, Mohammad Ali Ebadi, Hamed Farshbaf, and Iraj Nasoudi for their valuable insights.

## References

- ASTM. 1998. *Standard test method for identification and classification of dispersive clay soils by the pinhole test*. ASTM D4647-93(1998)e1. West Conshohocken, PA: ASTM.
- ASTM. 2000. *Standard test method for turbidity of water (withdrawn 2007)*. ASTM D1889. West Conshohocken, PA: ASTM.
- ASTM. 2003. *Standard test method for filterable and nonfilterable matter in water*. ASTM D5907. West Conshohocken, PA: ASTM.
- ASTM. 2011a. *Standard terminology relating to tissue engineered medical products*. ASTM F2312. West Conshohocken, PA: ASTM.
- ASTM. 2011b. *Standard test method for dispersive characteristics of clay soil by double hydrometer*. ASTM D4221. West Conshohocken, PA: ASTM.
- Correia dos Santos, R. N., L. M. M. S. Caldeira, and E. Maranha das Neves. 2017. "Factors limiting the progression of internal erosion in zoned dams: Flow limiting by an upstream material." *J. Geotech. Geoenvir. Eng.* 143 (1): 04016080. [https://doi.org/10.1061/\(ASCE\)GT.1943-5606.0001576](https://doi.org/10.1061/(ASCE)GT.1943-5606.0001576).
- Costa, L. M., and E. E. Alonso. 2009. "Predicting the behavior of an earth and rockfill dam under construction." *J. Geotech. Geoenvir. Eng.* 135 (7): 851–862. [https://doi.org/10.1061/\(ASCE\)GT.1943-5606.000058](https://doi.org/10.1061/(ASCE)GT.1943-5606.000058).
- Duncan, J. M., and C. Y. Chang. 1970. "Nonlinear analysis of stress and strain in soils." *J. Soil Mech. Found. Div.* 96 (5): 1629–1653.
- Fell, R., and J. J. Fry. 2013. "State of the art on the likelihood of internal erosion of dams and levees by means of testing." In *Erosion in geomechanics applied to dams and levees*. 1st ed. London: Wiley-ISTE.
- FEMA. 2011. *Filters for embankment dams: Best practices for design and construction*. Washington, DC: FEMA.
- Flores-Berrones, R., M. Ramírez-Reynaga, and E. J. Macari. 2011. "Internal erosion and rehabilitation of an earth-rock dam." *J. Geotech. Geoenviron. Eng.* 137 (2): 150–160. [https://doi.org/10.1061/\(ASCE\)GT.1943-5606.0000371](https://doi.org/10.1061/(ASCE)GT.1943-5606.0000371).
- Foster, M., R. Fell, and M. Spannagle. 2000a. "A method for assessing the relative likelihood of failure of embankment dams by piping." *Can. Geotech. J.* 37 (5): 1025–1061. <https://doi.org/10.1139/t00-029>.
- Foster, M., R. Fell, and M. Spannagle. 2000b. "The statistics of embankment dam failures and accidents." *Can. Geotech. J.* 37 (5): 1000–1024. <https://doi.org/10.1139/t00-030>.
- Garner, S. J., and R. J. Fannin. 2010. "Understanding internal erosion: A decade of research following a sinkhole event." *Hydropower Dams*. 17 (3): 93–98.
- Gillon, M. D. 2014. "Re-evaluation of internal erosion incidents at Matahina Dam, New Zealand." In *Internal erosion of dams and their foundations*, 123–140. Boca Raton, FL: CRC Press.
- Hajjalilue-Bonab, M., and S. K. Razavi. 2016. "A study of soil-nailed wall behaviour at limit states." *Proc. Inst. Civ. Eng. Ground Improv.* 169 (1): 64–76. <https://doi.org/10.1680/jgrim.14.00021>.
- Hunter, G., and R. Fell. 2003. *The deformation behaviour of embankment dams*. Sydney NSW, Australia: Univ. of New South Wales, School of Civil and Environmental Engineering.
- ICOLD (International Commission on Large Dams). 1994. *Embankment dams granular filter and drains*. Bulletin 5. Paris: ICOLD.
- Itasca. 2011. *Fast Lagrangian analysis of continua in 3 dimensions, user's guide*. FLAC3D V5.0. Minneapolis: Itasca Consulting Group.
- Kenney, T. C., and D. Lau. 1985. "Internal stability of granular filters." *Can. Geotech. J.* 22 (2): 215–225. <https://doi.org/10.1139/t85-029>.
- MacGregor, P., R. Fell, D. Stapledon, G. Bell, and M. Foster. 2014. *Geotechnical engineering of dams*. Boca Raton, FL: CRC Press.
- Moffat, R., and R. J. Fannin. 2011. "A hydromechanical relation governing internal stability of cohesionless soil." *Can. Geotech. J.* 48 (3): 413–424. <https://doi.org/10.1139/T10-070>.
- Nabavi, M. 1976. *An introduction to the geology of Iran*. [In Persian.] Tehran, Iran: Geological Survey of Iran Publication.
- Razavi, S. K., and M. H. Bonab. 2017. "Study of soil nailed wall under service loading condition." *Proc. Inst. Civ. Eng.-Geotech. Eng.* 170 (2): 161–174. <https://doi.org/10.1680/jgeen.16.00006>.
- Rönnqvist, H., and P. Viklander. 2014. "On the Kenney-Lau approach to internal stability evaluation of soils." *Geomaterials* 4 (4): 129. <https://doi.org/10.4236/gm.2014.44013>.
- Rönnqvist, H., P. Viklander, and S. Knutsson. 2017. "Experimental investigation of suffusion in dam core soils of glacial tills." *Geotech. Test. J.* 40 (3): 426–439. <https://doi.org/10.4236/gm.2014.44013>.
- Stark, T. D., and J. J. Vettel. 1991. "Effective stress hyperbolic stress-strain parameters for clay." *Geotech. Test. J.* 14 (2): 146–156. <https://doi.org/10.1520/GTJ10556J>.
- USBR (US Bureau of Reclamation). 2011. "Bureau of reclamation's embankment dams, design standards No. 13." Chap. 5 in *Protective filters*. Denver: US Dept. of the Interior, Bureau of Reclamation.
- Wan, C. F., and R. Fell. 2008. "Assessing the potential of internal instability and suffusion in embankment dams and their foundations." *J. Geotech. Geoenvir. Eng.* 134 (3): 401–407. [https://doi.org/10.1061/\(ASCE\)1090-0241\(2008\)134:3\(401\)](https://doi.org/10.1061/(ASCE)1090-0241(2008)134:3(401).
- Yea, G. G., T. H. Kim, J. H. Kim, and H. Y. Kim. 2013. "Rehabilitation of the core zone of an earth-fill dam." *J. Perform. Constr. Facil.* 27 (4): 485–495. [https://doi.org/10.1061/\(ASCE\)CF.1943-5509.0000335](https://doi.org/10.1061/(ASCE)CF.1943-5509.0000335).